

Quantum optical frequency up-conversion for polarisation entangled qubits: towards interconnected quantum information devices

FLORIAN KAISER,^{1,2,*} PANAGIOTIS VERGYRIS,^{1,3} ANTHONY MARTIN,^{1,4} DJEYLAN AKTAS,^{1,5} MARC P. DE MICHELI,^{1,6} OLIVIER ALIBART,¹ AND SÉBASTIEN TANZILLI¹

¹Université Côte d'Azur, CNRS, Institut de Physique de Nice (INPHYNI), UMR 7010, Parc Valrose, 06108 Nice Cedex 2, France

²Currently with the 3rd Institute of Physics, University of Stuttgart and Institute for Quantum Science and Technology IQST, 70569 Stuttgart, Germany

³Currently with Center for Life Nano Science@Sapienza, Istituto Italiano di Tecnologia, 00161 Rome, Italy

⁴Currently with the Group of Applied Physics, University of Geneva, Switzerland

⁵Currently with the Quantum Engineering Technology Labs, H. H. Wills Physics Laboratory and Department of Electrical and Electronic Engineering, University of Bristol, Bristol BS8 1FD, UK

⁶Deceased on July 10, 2019.

*f.kaiser@pi3.uni-stuttgart.de

Abstract: Realising a global quantum network requires combining individual strengths of different quantum systems to perform universal tasks, notably using flying and stationary qubits. However, transferring coherently quantum information between different systems is challenging as they usually feature different properties, notably in terms of operation wavelength and wavepacket. To circumvent this problem for quantum photonics systems, we demonstrate a polarisation-preserving quantum frequency conversion device in which telecom wavelength photons are converted to the near infrared, at which a variety of quantum memories operate. Our device is essentially free of noise which we demonstrate through near perfect single photon state transfer tomography and observation of high-fidelity entanglement after conversion. In addition, our guided-wave setup is robust, compact, and easily adaptable to other wavelengths. This approach therefore represents a major building block towards advantageously connecting quantum information systems based on light and matter.

© 2021 Optical Society of America under the terms of the [OSA Open Access Publishing Agreement](#)

1. Introduction

Quantum technologies have the potential to revolutionise the way information is processed and communicated [1, 2]. Quantum computers and simulators should permit to solve hard computational tasks and simulate complex systems, respectively more efficiently than classical ones [3, 4]. In quantum metrology, novel sensors achieve performances that are far beyond the capabilities of their classical counterparts [5, 6]. Quantum communication should bring absolute security in data exchange [7]. The future very likely lies in making those quantum technological pillars compatible with each other to combine individual system advantages. Although multi-functional quantum systems have already been demonstrated [8, 9], the usual situation today is that specific technologies are tailored for each application. One major obstacle in connecting various quantum systems lies in the wavelength discrepancy between different systems. For example, photons are generally preferred for quantum communication purposes [10–12], and minimal loss in fibre networks is obtained at telecom wavelengths ($\lambda \sim 1.55 \mu\text{m}$). On the other hand, quantum computation, storage, and metrology tasks are usually performed with matter

based systems that interact with wavelengths ranging from the visible to the near infrared band ($\lambda \sim 600 - 900$ nm) [13–15].

To bridge this gap, the solution lies in *quantum interfaces* able to coherently convert photons back and forth between the different wavelength bands [16]. Such wavelength conversion interfaces are compatible with essentially all photonic observables, *e.g.* energy-time [16, 17], time-bin [18–21], orbital angular momentum [22, 23], squeezed states of light [24], and polarisation [25–30]. Concerning the very popular polarisation observable, a high-efficiency and versatile up-converter from telecom to the quantum memory band is still missing. One attempt based on three-wave mixing in nonlinear crystals showed up-conversion from 810 nm to 532 nm, but the reported conversion efficiency is $\sim 0.04\%$ [25]. Down-conversion experiments showed however, that higher efficiencies in the few 10 percent range should be feasible [26–30].

Our work provides a decisive step forward in this regard. We demonstrate a novel quantum interface in which single photons are converted via sum frequency generation (SFG) in nonlinear crystals from 1560 nm to 795 nm. Key features of our approach are a high conversion efficiency and the preservation of polarisation quantum states with high fidelity. We choose a design based on nonlinear guided-wave optics to increase robustness and facilitate integration into existing standard systems. Furthermore, our device is essentially noise-free over a spectral bandwidth compatible with stationary quantum systems based on hot and cold atomic ensembles, as well as solid state quantum memories [13]. Therefore, our work represent a significant step towards interconnecting the pillars of quantum communication, storage, and computation.

2. Setup

The physical realisation of our quantum interface is depicted in Fig. 1. The target is to convert single photons from 1560 nm to 795 nm via SFG with a 1621 nm pump laser. Single photons and pump laser are combined into the same fibre using a standard telecom wavelength division multiplexer (WDM). Conversion takes place in two 3.8 cm long periodically poled lithium niobate waveguides (PPLN/W_{1,2}). One PPLN/W is placed in each arm of a Mach-Zehnder type interferometer made of polarisation maintaining fibres and polarising beam splitters (PBS_{1,2}) at the in- and output. PBS₁ splits up light into horizontally and vertically polarised components, subsequently propagating in the upper and lower arms, respectively. After wavelength conversion in the PPLN/Ws, the polarisation components are recombined into the same spatial mode at PBS₂. In both crystals, we choose to exploit the type-0 interaction which is associated with the largest obtainable nonlinear coefficient. Note that this interaction necessitates that all light fields are vertically polarised inside the crystal [31], which is why we rotate PPLN/W₁ by 90° around the light propagation axis.

To ensure that the wavelength conversion process does not deteriorate the polarisation state between the input and output photon, two requirements need to be satisfied [26–30]. First, the conversion efficiency in both arms needs to be equalised; second, the optical phase difference between upper and lower arms needs to be zero to avoid polarisation state rotation. We fulfil the first condition by rotating the polarisation of the 1621 nm laser power with a polarisation controller (PC) until each PPLN/W receives ~ 100 mW of optical power. The second condition necessitates an active interferometer phase stabilisation system. We implement it by *recycling* the spurious emission at 810 nm originating from residual frequency doubling of the 1621 nm pump laser. We use a dichroic mirror to separate this light from the desired photons at 795 nm. After projecting the 810 nm photons into the diagonal basis, we observe phase-dependent interference fringes. A piezoelectric fibre stretcher in one arm of the interferometer is then used to maintain the phase stable.

Conversion devices based on PPLN show generally strong and broadband Raman scattering at ~ 250 cm⁻¹ and ~ 630 cm⁻¹ [32, 33]. The resulting photonic noise is detrimental for quantum applications based on single photons and usually necessitates several filtering stages. In our

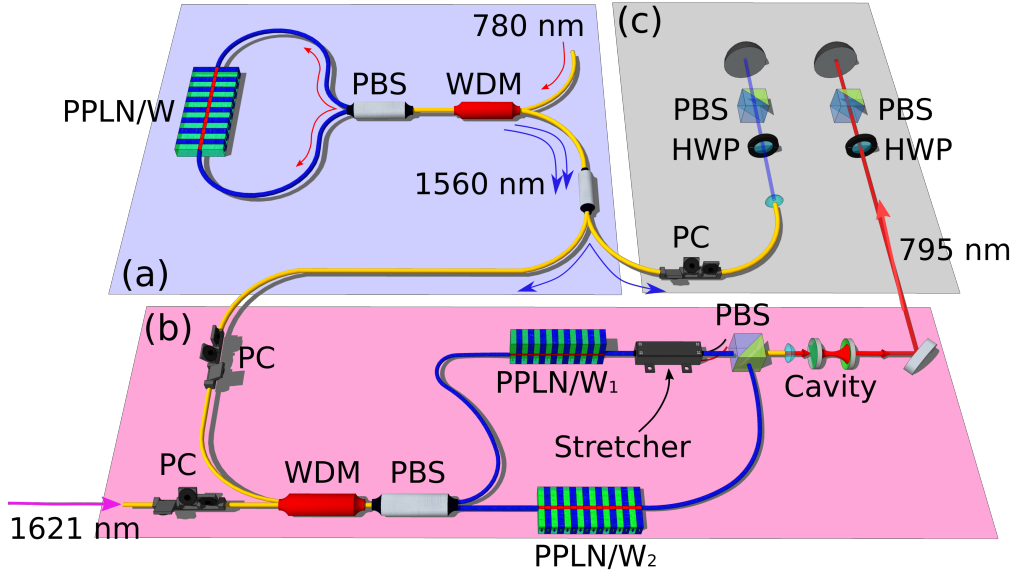


Fig. 1. Experimental scheme. (a) Polarization entangled photon pair source based in a fiber-based nonlinear Sagnac loop. Photons pairs are created by SPDC into a type-0 PPLN/w at the degeneracy wavelengths 1560 nm. (b) Polarization-coherent up-conversion setup. Signal photons (1560 nm) and pump laser (1621 nm) are combined into a nonlinear fiber-based MZI. The horizontally (vertically) polarization components of the input are up-converted in the top (bottom) waveguide to a horizontally (vertically) photon, i.e. mode, at 795 nm. (c) Polarization analysis and Bell state measurements apparatus. The entangled pair, composed of the 1560 nm and 795 nm photons, are sent to two polarization state analyzers. The polarization rotation is implemented using two HWP optimized at their corresponding wavelengths and projected onto a beam splitter. The photons are fiber-coupled and detected by single photon counting modules permitting the registration of coincidence events.

experiment, we actually choose deliberately to operate in a worst-case scenario to demonstrate the suitability of our filtering stage. In PPLN, the first anti-Stokes emission peak of the 1621 nm pump laser is situated at ~ 1560 nm, *i.e.* overlaying with the wavelength of the photons that we want to convert. To filter out Raman noise, we use a home-made hemispherical cavity at 795 nm with a free spectral range of 150 GHz. This way, we ensure that there is only one transmission peak within the spectral conversion bandwidth of our PPLN/Ws (40 – 44 GHz). We choose a cavity transmission bandwidth of ~ 250 MHz to be compatible with the absorption of quantum systems based on atomic vapours and solid state quantum memories [13]. Thanks to the narrow transmission bandwidth, wavelength converted anti-Stokes photons within the spectral conversion bandwidth are strongly suppressed by about two orders of magnitude. We further use a 795 nm reference laser to implement an active cavity stabilisation system with a temporal duty cycle of 6%. Finally, before coupling light back into an optical fibre, we employ a 800 ± 20 nm bandpass filter to suppress light at 540 nm originating from parasitic frequency tripling inside the PPLN/Ws.

3. Results

In a first step, we perform a semi-classical characterisation of our interface device. For this, we simulate a source of diagonally polarised single photons by carving 10 ns long pulses out of a

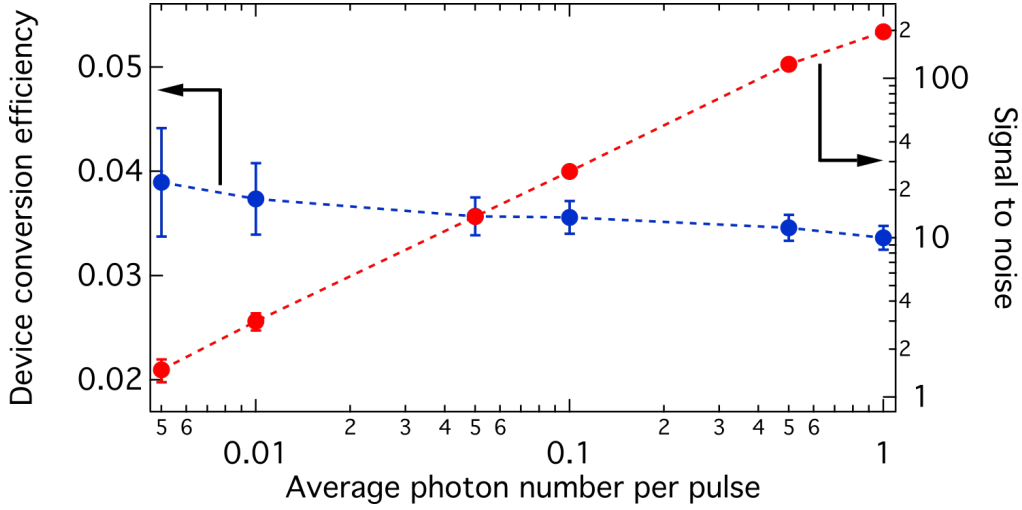


Fig. 2. Device conversion efficiency η (blue dots) and associated SNR (red dots) as a function of the average number of photons per laser pulse \bar{n} . Dashed lines are guides to the eye.

1560 nm continuous wave laser. Via a digital attenuator, we then adjust the average number of photons per pulse in the range of $\bar{n} = 0 - 1$. After the interface, photons arriving within a 10 ns window are detected using a silicon single photon detector (SPD) with 50% efficiency and a free-running dark count rate of $\sim 120 \text{ s}^{-1}$.

Fig. 2 shows the wavelength conversion efficiency of the full device (η) and the obtained signal-to-noise ratio (SNR) as a function of \bar{n} . From the data, we infer $\eta = 3.6 \pm 0.2\%$, which is about two orders of magnitude higher than demonstrated previously [25]. To infer how our efficiency could be further improved, we analyse the optical loss of our setup. In total, we measure 8.8 dB, broken down as follows: 3 dB from the WDM to the PPLN/Ws; 3.7 dB from PPLN/Ws to the cavity; 1.1 dB inside the cavity including its stabilisation system; and 1 dB from cavity into the optical fibre towards the SPD. Thus, we estimate the internal conversion efficiency of the PPLN/Ws to be $27.3 \pm 1.5\%$. Concerning SNR measurements, our filtering stage proves to be effective as we achieve high levels even at low \bar{n} . From a linear fit to the recorded data, we obtain $\text{SNR} = 243(1) \cdot \bar{n}$.

In a second step, we perform single photon polarisation state tomography to demonstrate that our quantum interface does not alter the quantum state [34–36]. Setting $\bar{n} = 0.5$ we generate the six basis polarisation states $|H\rangle$, $|V\rangle$, $\frac{|H\rangle+|V\rangle}{\sqrt{2}} \equiv |D\rangle$, $\frac{|H\rangle-|V\rangle}{\sqrt{2}} \equiv |A\rangle$, $\frac{|H\rangle+i|V\rangle}{\sqrt{2}} \equiv |R\rangle$, $\frac{|H\rangle-i|V\rangle}{\sqrt{2}} \equiv |L\rangle$ at 1560 nm with fidelities of ~ 0.99 . Here, $|H\rangle$ and $|V\rangle$ denote horizontally and vertically photon polarisations, respectively. These photons are then wavelength converted and their polarisation state is measured using a quarter wave plate (QWP), a half wave plate (HWP), and a PBS. Fig. 3 shows the detected quantum states at 795 nm. From the data, we compute quantum state fidelities of $\mathcal{F}_{|H\rangle} = 0.98$, $\mathcal{F}_{|V\rangle} = 0.98$, $\mathcal{F}_{|D\rangle} = 0.96$, $\mathcal{F}_{|A\rangle} = 0.98$, $\mathcal{F}_{|R\rangle} = 0.94$, and $\mathcal{F}_{|L\rangle} = 0.95$, with typical error bars of ± 0.01 . The origin of the fidelity decrease will be discussed later in this section.

In the final step, we proceed to wavelength conversion of polarisation entangled photons to demonstrate the polarisation-insensitivity of our device in a universal manner [16]. Here, we use a previously developed source based on a nonlinear Sagnac interferometer (see Fig. 1a) [37]. Photon pairs are generated at 1560 nm in the maximally entangled polarisation Bell state $|\psi\rangle = (|H\rangle|H\rangle + |V\rangle|V\rangle)/\sqrt{2}$ with an initial fidelity of $\mathcal{F}_i = 0.989 \pm 0.002$. After the source, photon pairs are split up probabilistically at a fibre beam-splitter. The photon that is not

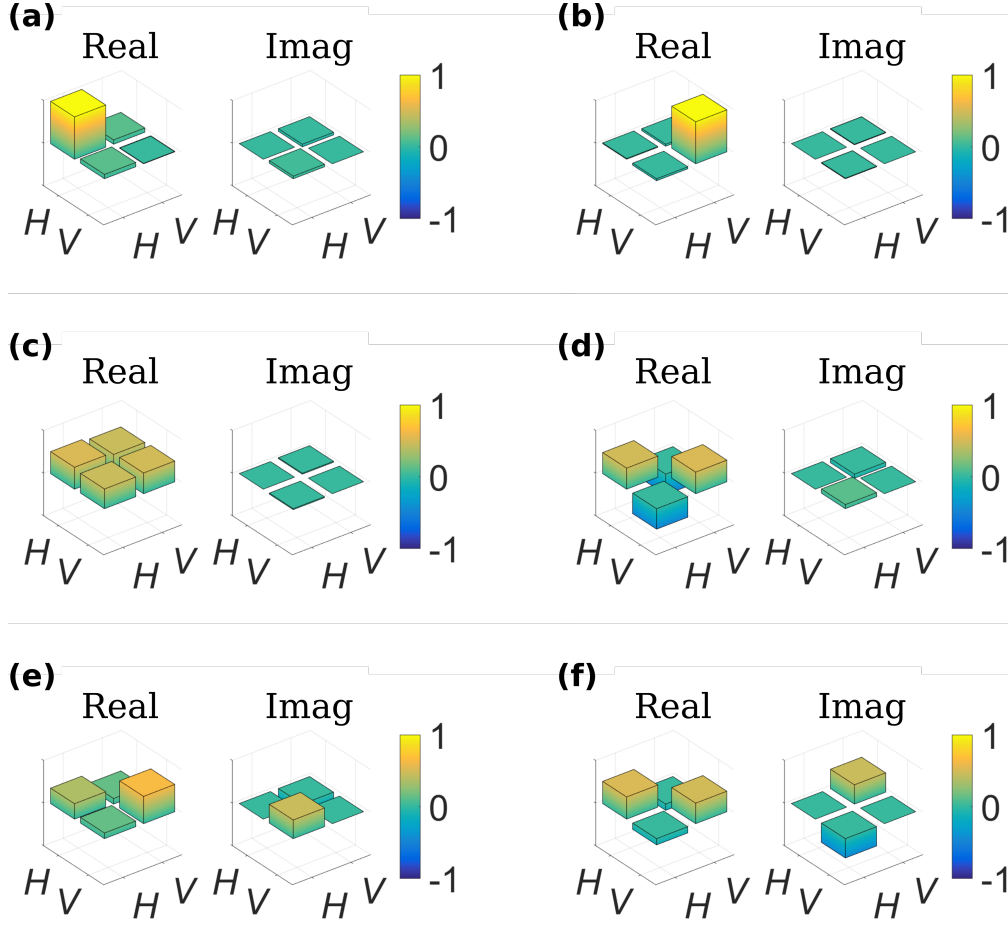


Fig. 3. Real and imaginary parts of the single photon polarisation state tomography after wavelength conversion to 795 nm. The 1560 nm input states are (a) $|H\rangle$, (b) $|V\rangle$, (c) $|D\rangle$, (d) $|A\rangle$, (e) $|R\rangle$, and (f) $|L\rangle$, respectively.

wavelength converted is filtered down to a spectral bandwidth of 500 MHz with a phase-shifted fibre Bragg grating to roughly match the bandwidth of the noise-reduction filter cavity (250 MHz). The photon's polarisation state is subsequently detected using a half-wave plate (HWP), a PBS, followed by a superconducting nanowire single photon detector (SNSPD, IDQ281) with 50% efficiency and a free-running dark count rate of 250 s^{-1} . The other photon is sent to the interface, wavelength converted, and its polarisation state is measured using a HWP, PBS, and a SPD. Both detectors are connected to a time-to-digital converter, allowing to infer two-photon coincidence events. Fig. 4 shows the two photon interference fringes acquired when the polarisation state of the 795 nm is projected onto $|H\rangle$ and $|D\rangle$, respectively, and the polarisation state of the non-converted photon is rotated continuously. We measure net interference fringe visibilities of $\mathcal{V}_{|H\rangle} = 94.9 \pm 0.2\%$ and $\mathcal{V}_{|D\rangle} = 95.2 \pm 0.2\%$. From the average visibility $\bar{\mathcal{V}}$, we estimate a quantum state fidelity of $\mathcal{F}_{\text{net}} = (\bar{\mathcal{V}} + 1) / 2 = 0.976 \pm 0.001$. Without subtracting noise terms, we infer a raw fidelity of $\mathcal{F}_{\text{I,raw}} = 0.945 \pm 0.001$. The total 5.4% drop in fidelity compared to \mathcal{F}_{I} has three main origins. From $\mathcal{F}_{\text{I,net}}$, we conclude that 1.3% degradation is due to non-optimal setup alignment, *i.e.* non-equilibrated conversion efficiencies between the two PPLN/Ws and phase fluctuations inside the interferometer. By performing a measurement with the 1621 nm

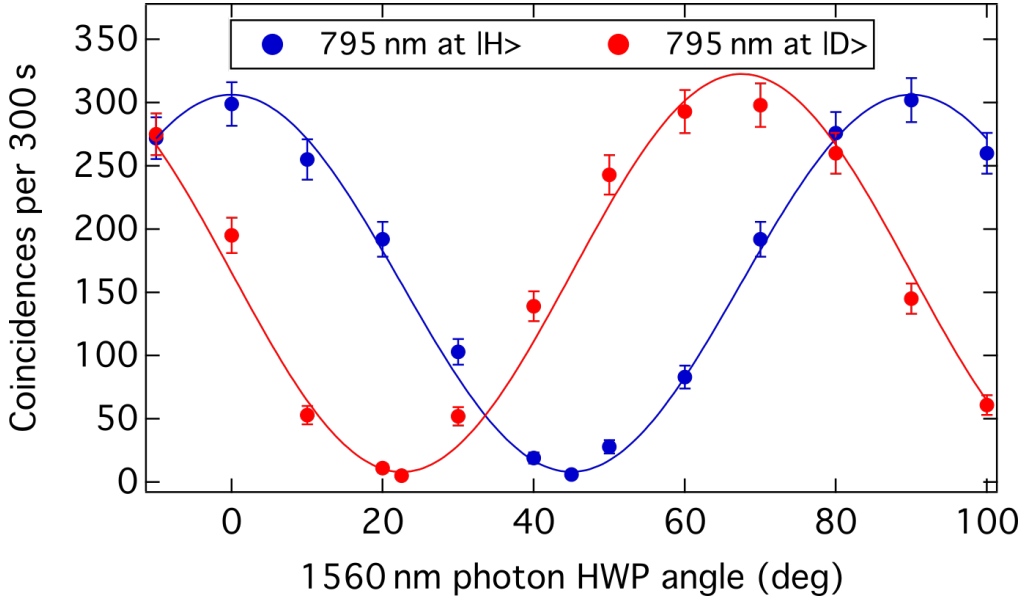


Fig. 4. Two photon coincidences as a function of the 1560 nm HWP angle. The polarisation state of the 795 nm is being projected onto $|H\rangle$ (blue dots) and $|D\rangle$ (red dots), respectively. Lines are sinusoidal fits to the data from which we extract fringe visibilities of $\mathcal{V}_{|H\rangle} = 94.9 \pm 0.2\%$ and $\mathcal{V}_{|D\rangle} = 95.2 \pm 0.2\%$, respectively.

pump laser being switched off, we infer that 1.6% loss in fidelity is due to detector dark counts (effectively 0.02 noise photons per second after coincidence gating). The remaining 1.5% come from photonic noise due to Raman scattering.

Our current quantum state transfer fidelity is therefore $\mathcal{F}_{\text{trans}} = \mathcal{F}_{\text{f,raw}}/\mathcal{F}_{\text{i}} = 0.956 \pm 0.002$. Through technical improvements, such as better setup alignment and employing ultra low noise detectors, an optimal fidelity $\mathcal{F}_{\text{trans}}^* = 0.985$ could be reached. Finally, we mention again that we deliberately chose to operate our experiment in worst-case scenario regarding photonic noise. For *optimal* wavelength combinations, *i.e.* conversion from 1530 nm to 795 nm, photonic noise is almost two orders of magnitude lower [32], such that near unit transfer fidelities are definitely realisable. Alternatively, the filter cavity could be removed, thus increasing the the full device conversion efficiency by 1.1 dB.

4. Conclusion and discussion

We have demonstrated polarisation state preserving quantum frequency conversion from 1560 nm to 795 nm.

In our setup, we achieved a total device conversion efficiency of 3.6%, which could be increased by a factor 3 to 4 with a more powerful 1621 nm pump laser. Another twofold improvement is feasible through reducing optical losses, *e.g.* by splicing all fibres and employing custom optical filters and dichroic mirrors.

Although we chose to operate in a worst-case scenario concerning photonic noise induced by Raman scattering, we show excellent signal-to-noise thanks to a filter cavity stage. This allowed us to wavelength convert one photon out of an entangled pair with more than 95% fidelity, and pathways towards achieving near-unit fidelities have been outlined.

Since our device is almost exclusively based on fibre and guided-wave technology, integration into existing systems is greatly simplified. In this perspective, we mention that essentially no

efforts have to be made to establish and maintain a good mode overlap between the single photons and the pump laser which further increases robustness. Further stability improvements could be made with a fully integrated QFC device, and promising efforts in this direction have recently been demonstrated, *e.g.* on-chip combination of PPLN/Ws and PBS [38] or high-rejection spectral filtering stages [39].

We also stress that our particular choice of wavelengths and the adapted transmission bandwidth of the filter cavity makes our setup ready to be used in a quantum repeater based network. Here, the idea is to distribute 1560 nm entangled photons in a fibre network, convert them to 795 nm, and store them in a (hot) rubidium atom based quantum memory. Cold atom memories with absorption bandwidth in the few MHz range can also be addressed, however, the filter cavity bandwidth should be reduced in this case to guarantee a high signal-to-noise ratio.

By combining our work with recently demonstrated downconversion interfaces [26–29], we are now a significant step closer to a universal quantum network based on frequency conversion back and forth between quantum systems based on light and matter.

Funding

Foundation Simone & Cino Del Duca; European Commission (FP7-ITN PICQUE project, grant agreement No 608062); Agence Nationale de la Recherche (ANR) (e-QUANET grant ANR-09-BLAN-0333-01, CONNEQT grant ANR-EMMA-002-01, INQCA grant ANR-14-CE26-0038, and SPOCQ grant ANR-14-CE32-0019, Quantum@UCA grant ANR-15-IDEX-01); iXCore Research Foundation; French government (Université Côte d’Azur UCA-JEDI project); European Union and Région PACA (OPTIMAL project via Fond Européen de Développement Régional, FEDER).

Disclosures

The authors declare that there are no conflicts of interest related to this article.

References

1. M. Mohseni, P. Read, H. Neven, S. Boixo, V. Denchev, R. Babbush, A. Fowler, V. Smelyanskiy, and J. Martinis, “Commercialize quantum technologies in five years,” *Nature* **543**, 171–174 (2017).
2. M. F. Riedel, D. Binosi, R. Thew, and T. Calarco, “The European quantum technologies flagship programme,” *Quantum Sci. Technol.* **2**, 030501 (2017).
3. A. Steane, “Quantum computing,” *Rep. Prog. Phys.* **61**, 117–173 (1998).
4. T. D. Ladd, F. Jelezko, R. Laflamme, Y. Nakamura, C. Monroe, and J. L. O’Brien, “Quantum computers,” *Nature* **464**, 45–53 (2010).
5. V. Giovannetti, S. Lloyd, and L. Maccone, “Advances in quantum metrology,” *Nat. Photon.* **5**, 222–229 (2011).
6. C. L. Degen, F. Reinhard, and P. Cappellaro, “Quantum sensing,” *Rev. Mod. Phys.* **89**, 035002 (2017).
7. N. Gisin, G. Ribordy, W. Tittel, and H. Zbinden, “Quantum cryptography,” *Rev. Mod. Phys.* **74**, 145–195 (2002).
8. S. Barz, E. Kashefi, A. Broadbent, J. F. Fitzsimons, A. Zeilinger, and P. Walther, “Demonstration of blind quantum computing,” *Science* **335**, 303–308 (2012).
9. J. F. Fitzsimons, “Private quantum computation: an introduction to blind quantum computing and related protocols,” *npj Quantum Inform.* **3**, 23 (2017).
10. R. Valivarthi, M. Puigibert, Q. Zhou, G. H. Aguilar, V. B. Verma, F. Marsili, M. D. Shaw, S. W. Nam, D. Oblak, and W. Tittel, “Quantum teleportation across a metropolitan fibre network,” *Nat. Photon.* **10**, 676–680 (2016).
11. Q.-C. Sun, Y.-L. Mao, S.-J. Chen, W. Zhang, Y.-F. Jiang, Y.-B. Zhang, W.-J. Zhang, S. Miki, T. Yamashita, H. Terai, X. Jiang, T.-Y. Chen, L.-X. You, X.-F. Chen, Z. Wang, J.-Y. Fan, Q. Zhang, and J.-W. Pan, “Quantum teleportation with independent sources and prior entanglement distribution over a network,” *Nat. Photon.* **10**, 671–675 (2016).
12. H.-L. Yin, T.-Y. Chen, Z.-W. Yu, H. Liu, L.-X. You, Y.-H. Zhou, S.-J. Chen, Y. Mao, M.-Q. Huang, W.-J. Zhang, H. Chen, M. J. Li, D. Nolan, F. Zhou, X. Jiang, Z. Wang, Q. Zhang, X.-B. Wang, and J.-W. Pan, “Measurement-device-independent quantum key distribution over a 404 km optical fiber,” *Phys. Rev. Lett.* **117**, 190501 (2016).
13. A. I. Lvovsky, B. C. Sanders, and W. Tittel, “Optical quantum memory,” *Nat. Photon.* **3**, 706–714 (2009).
14. F. Bussières, N. Sangouard, M. Afzelius, H. de Riedmatten, C. Simon, and W. Tittel, “Prospective applications of optical quantum memories,” *J. Mod. Opt.* **60**, 1519–1537 (2013).
15. K. Heshami, D. G. England, P. C. Humphreys, P. J. Bustard, V. M. Acosta, J. Nunn, and B. J. Sussman, “Quantum memories: emerging applications and recent advances,” *J. Mod. Opt.* **63**, 2005–2028 (2016).

16. S. Tanzilli, W. Tittel, M. Halder, O. Alibart, P. Baldi, N. Gisin, and H. Zbinden, "A photonic quantum information interface," *Nature* **437**, 116–120 (2005).
17. A. Lenhard, J. Brito, M. Bock, C. Becher, and J. Eschner, "Coherence and entanglement preservation of frequency-converted heralded single photons," *Opt. Express* **25**, 11187–11199 (2017).
18. A. P. VanDevender and P. G. Kwiat, "Quantum transduction via frequency upconversion," *J. Opt. Soc. Am. B* **24**, 295–299 (2007).
19. Y. O. Dudin, A. G. Radnaev, R. Zhao, J. Z. Blumoff, T. A. B. Kennedy, and A. Kuzmich, "Entanglement of light-shift compensated atomic spin waves with telecom light," *Phys. Rev. Lett.* **105**, 260502 (2010).
20. R. Ikuta, Y. Kusaka, T. Kitano, H. Kato, T. Yamamoto, M. Koashi, and N. Imoto, "Wide-band quantum interface for visible-to-telecommunication wavelength conversion," *Nat. Commun.* **2**, 537 (2011).
21. N. Maring, P. Farrera, K. Kutluer, G. Heinze, and H. de Riedmatten, "Photonic quantum state transfer between a cold atomic gas and a crystal," *Nature* **551**, 485–488 (2017).
22. Z.-Y. Zhou, S.-L. Liu, Y. Li, D.-S. Ding, W. Zhang, S. Shi, M.-X. Dong, B.-S. Shi, and G.-C. Guo, "Orbital angular momentum-entanglement frequency transducer," *Phys. Rev. Lett.* **117**, 103601 (2016).
23. Z.-Y. Zhou, Y. Li, D.-S. Ding, W. Zhang, S. Shi, B.-S. Shi, and G.-C. Guo, "Orbital angular momentum photonic quantum interface," *Light Sci. Appl.* **5**, e16019 (2016).
24. C. Baune, J. Gniesmer, S. Kocsis, C. E. Vollmer, P. Zell, J. Fiurášek, and R. Schnabel, "Unconditional entanglement interface for quantum networks," *Phys. Rev. A* **93**, 010302 (2016).
25. S. Ramelow, A. Fedrizzi, A. Poppe, N. K. Langford, and A. Zeilinger, "Polarization-entanglement-conserving frequency conversion of photons," *Phys. Rev. A* **85**, 013845 (2012).
26. V. Krutyanskiy, M. Meraner, J. Schupp, and B. P. Lanyon, "Polarisation-preserving photon frequency conversion from a trapped-ion-compatible wavelength to the telecom C-band," *Appl. Phys. B* **123**, 228 (2017).
27. R. Ikuta, T. Kobayashi, T. Kawakami, S. Miki, M. Yabuno, T. Yamashita, H. Terai, M. Koashi, T. Mukai, T. Yamamoto, and N. Imoto, "Polarization insensitive frequency conversion for an atom-photon entanglement distribution via a telecom network," *Nat. Commun.* **9**, 1997 (2018).
28. M. Bock, P. Eich, S. Kucera, M. Kreis, A. Lenhard, C. Becher, and J. Eschner, "High-fidelity entanglement between a trapped ion and a telecom photon via quantum frequency conversion," *Nat. Commun.* **9**, 1998 (2018).
29. N. Maring, D. Lago-Rivera, A. Lenhard, G. Heinze, and H. de Riedmatten, "Quantum frequency conversion of memory-compatible single photons from 606 nm to the telecom c-band," *Optica* **5**, 507–513 (2018).
30. V. Krutyanskiy, M. Meraner, J. Schupp, V. Krcmarsky, H. Hainzer, and B. P. Lanyon, "Light-matter entanglement over 50 km of optical fibre," *arXiv:1901.06317v1* (2019).
31. S. Tanzilli, W. Tittel, H. De Riedmatten, H. Zbinden, P. Baldi, M. DeMicheli, D. Ostrowsky, and N. Gisin, "PPLN waveguide for quantum communication," *Eur. Phys. J. D* **18**, 155–160 (2002).
32. J. S. Pelc, L. Ma, C. R. Phillips, Q. Zhang, C. Langrock, O. Slattery, X. Tang, and M. M. Fejer, "Long-wavelength-pumped upconversion single-photon detector at 1550 nm: performance and noise analysis," *Opt. Express* **19**, 21445–21456 (2011).
33. F. Kaiser, A. Issautier, L. A. Ngah, D. Aktas, T. Delord, and S. Tanzilli, "Toward Continuous-Wave Regime Teleportation for Light Matter Quantum Relay Stations," *IEEE J. Sel. Top. Quantum Electron* **21**, 69–77 (2015).
34. D. F. V. James, P. G. Kwiat, W. J. Munro, and A. G. White, "Measurement of qubits," *Phys. Rev. A* **64**, 052312 (2001).
35. J. Altepeter, E. Jeffrey, and P. Kwiat, "Photonic state tomography," *Adv. Atom. Mol. Opt. Phys.* **52**, 105–159 (2005).
36. O. Bayraktar, M. Swillo, C. Canalias, and G. Björk, "Quantum-polarization state tomography," *Phys. Rev. A* **94**, 020105 (2016).
37. P. Vergyris, F. Kaiser, E. Gouzien, G. Sauder, T. Lunghi, and S. Tanzilli, "Fully guided-wave photon pair source for quantum applications," *Quantum Sci. Technol.* **2**, 024007 (2017).
38. L. Sansoni, K. H. Luo, C. Eigner, R. Ricken, V. Quiring, H. Herrmann, and C. Silberhorn, "A two-channel, spectrally degenerate polarization entangled source on chip," *npj Quantum Inform.* **3**, 5 (2018).
39. D. Pérez-Galacho, C. Alonso-Ramos, F. Mazeas, X. L. Roux, D. Oser, W. Zhang, D. Marris-Morini, L. Labonté, S. Tanzilli, É. Cassan, and L. Vivien, "Optical pump-rejection filter based on silicon sub-wavelength engineered photonic structures," *Opt. Lett.* **42**, 1468–1471 (2017).